Synthesis and Study of the Physicochemical Properties of a Hybrid Species: Iron Phthalocyanine–Silver Nanoparticles

Lassané Tarpaga, Bintou Sessouma, Seydou Ouédraogo, V. Collière, Mabinty Bayo-Bangoura, Catherine Amiens, Karifa Bayo

Synthesis and study of the physicochemical properties of a hybrid species: iron phthalocyanine-silver nanoparticles

Lassané Tarpaga*[1,2], Bintou Sessouma[1], Seydou Ouédraogo[1], Vincent Colliere[2], Mabinty Bayo-Bangoura[1], Catherine Amiens[2, 3], Karifa Bayo[1]

1. Laboratoire de Chimie Moléculaire et des Matériaux, Université Joseph KI-ZERBO, 03 BP 7021 Ouagadougou 03, Burkina Faso. lassane.tarpaga@ujkz.bf
2. CNRS, LCC (Laboratoire de Chimie de Coordination), 205 Route de Narbonne, BP 44099, F-31077 Toulouse Cedex 4, France.
3. Université de Toulouse, UPS, INPT, F-31077 Toulouse Cedex 4, France

Abstract

This article reports a strategy to synthesize a hybrid species made of iron phthalocyanine (FePc) grafted to the surface of silver nanoparticles. The affinity between sulfur and silver on the one hand, and the aptitude of the FePc complex to bind pyridine axially on the other, allowed us to use thiopyridine as a linker between the two entities. The hybrid species, isolated in the solid form for the first time, has been characterized by optical and vibrational spectroscopy, and by transmission electron microscopy. These studies confirm the good aptitude of the linker to connect the FePc to the silver nanoparticles.

Keywords:

iron phthalocyanine, silver nanoparticles, optical and vibrational spectroscopies, transmission electron microscopy

1. Introduction

Metallophthalocyanines (MPcs) are macrocyclic molecules made up of four benzopyrrole groups linked by nitrogens (see a typical example in **Scheme** 1). These compounds exhibit remarkable optical properties due to their conjugated π system. They absorb in the 200 to 900 nm range with an absorption maximum between 650 and 700 nm [1]. Since their discovery in 1907, their applications range from health sciences to electronics and to their traditional use as dyes and pigments [2 -13].

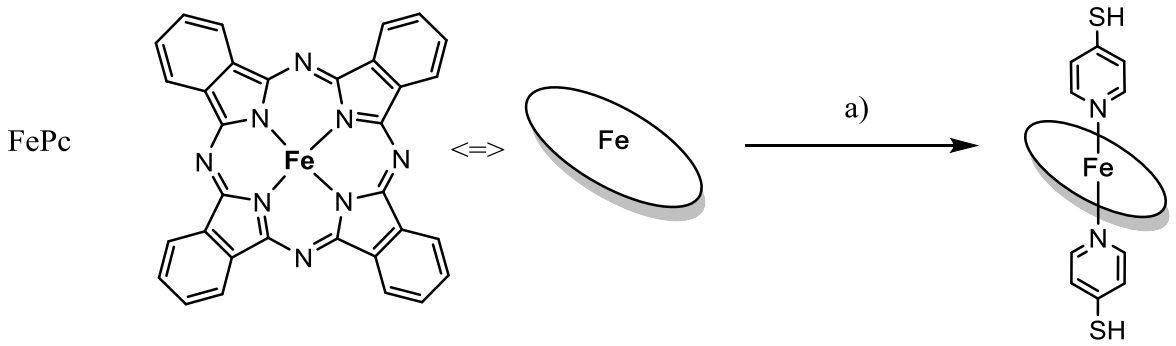

Scheme 1. Structure of a metallophthalocyanine illustrated in the case of Fe (FePc) and schematic representation used in the following of the paper, with reaction path followed to check the reactivity with 4-thiopyridine. a) acetonitrile, 4-thiopyridine (10 equiv.), reflux, 15 h.

Over the past 20 years, a renewed interest in these complexes has been triggered by the possibility of associating them with nanoparticles [14-18].

Among the nanoparticles of interest, silver nanoparticles (AgNPs) exhibit interesting intrinsic physical properties linked to their size: optical properties, high specific surface area and high surface reactivity, including strong redox activity. In relation to this redox activity, they are widely exploited for their antibacterial and antifungal properties [19-21]. Indeed, one of the reasons for their bactericidal effect was demonstrated to be the oxidative release of silver ions. These ions can produce Reactive Oxygen Species (ROS) through reaction with dissolved oxygen then affecting DNA, cell membrane and also membrane proteins. They can also interact with membrane proteins and DNA affecting their proper functioning. [22-24] Association of these nanoparticles with a photosensitizer, such as a metallophthalocyanine, is interesting because the complex can play the role of a light collecting antenna and thus the nanoparticles, where these complexes are locally concentrated, should more easily and gradually release Ag^+ ions.

This association is most often made at the periphery of the phthalocyanine macrocycle through -SH, -NH_2, -COOH groups, etc. The resulting hybrid species often aggregate which limits their field of application in solution [14-18].

In order to circumvent this problem, new compounds have been designed and synthesized by Masilela N and al. [25] by coordinating a Zn phthalocyanine (ZnPc) on the surface of AgNPs stabilized by 4-thiopyridine ligands. Their results show an improvement in the antibacterial activity of the hybrids compared to the nanoparticles alone. However, the exact structure of these hybrid species is poorly known. The authors suggest that in these compounds, the Zn^{2+} metal ion of the complex interacts with the nitrogen doublet of thiopyridine previously attached to the surface of the particle through sulfur. However, the study by Ogunsipe A [26] on ZnPc carrying pyridine axial ligands shows that these only interact with Zn through weak interactions. Indeed, these interactions are no longer observed upon solubilization of these complexes (in DMSO, DMF and Pyridine). This can be explained by the d^{10} electronic structure of the Zn^{2+} ion. The electron microscopy images obtained by Masilela N and al. show the formation of aggregates of particles probably attesting the lability of the 4-thiopyridine ligand towards ZnPc.

On the hypothesis that a more robust metal phthalocyanine / AgNPs hybrid might improve the synergy between the two components and afford still better antibacterial properties, we decided to investigate the coupling of FePc which present similar optical properties but different coordinating ones. Indeed, since the Fe^{2+} cation of the iron phthalocyanine (FePc) has accessible and partially filled “d” orbitals, it is likely to accept ligands in the apical position and bind them more strongly than the Zn^{2+} cation in ZnPc. In fact, many studies have been carried out on the binding of ligands (pyridines, thiols, phosphorus, etc.) in an axial position on the FePc complexes [27-29]. Our previous work [29, 30] has shown that the charge transfer band observed on the electron absorption spectra of FePc-ligand complexes is a clear indication of the coordination of pyridine ligands in the axial position.

We now report the successful synthesis and characterization of a stable hybrid species consisting of a AgNP functionalized on its surface by iron phthalocyanines through a 4-thiopyridine (4SHPy) linker. In other words, the association between the phthalocyanine macrocycles and the AgNP here occurs through the central metal (iron) and not at the periphery of the macrocycle through a coordination bond that should be stronger than in the ZnPc/AgNPs hybrid systems.

First, we checked the reactivity of the 4SHPy linker with the FePc complex and with the AgNPs. before preparing stable colloidal solutions of the hybrid species which could then be

isolated in the solid form for the first time. Characterization by a combination of spectroscopic techniques and transmission electron microscopy confirmed the success of our approach.

2. Experimental.

2. 1. Materials

Phtalonitrile (99.99%), iron (II) sulfate heptahydrate (> 99%), sodium hydroxide (> 98%), 4-mercaptopyridine (95%), nitrobenzene (> 99%), ethanol (> 99.9%), methanol (> 99.9%), acetone (> 99.9%), hydrochloric acid (> 99%)) and DMSO (> 99.9%) were obtained from Aldrich while silver nitrate (> 98%), ethylenediaminetetramethylenephosphonic acid (EDTMP, > 99%) and commercial ammonia solution (> 98%) were received from Alfa Aesar. All reagents and solvents were used without further purification. Ultrapure water (18.2 MΩ) used for the preparation of AgNPs was produced by a Milli-Q Millipore system.

2.2. Synthesis

2.2.1. Preparation of iron phthalocyanine (FePc). FePc was prepared and purified according to an already published procedure from our group [27, 30].

2.2.2. Preparation of complex FePc(4SHPy)$_2$. A mixture of 20 mg ($3.52\ 10^{-5}$ mol) of FePc and excess 4SHPy ligand ($3.52\ 10^{-4}$ mol) in 30 mL of acetonitrile was brought to reflux for 15 hours in the air. After filtration, the isolated green solid was washed with Milli-Q water and ethanol and then air dried (yield: 90%). [Cal: C/N = 3.5; H/N = 0.17; C/S = 13.86 and Exp: C/N = 3.55; H/N = 0.14; C/S = 15.6].

2.2.3. Preparation of silver nanoparticles (AgNPs). The AgNPs were prepared following the method described by Chaikin Y and al. [31]: 25 mL (1.23 mM) of an aqueous solution of $AgNO_3$, adjusted to pH = 8.5 by dropwise addition of concentrated ammonia, was placed in a two-necked flask (50 mL) and heated to boiling for 10 min. To the boiling aqueous solution of $AgNO_3$, kept under vigorous stirring, 160 µL of an aqueous solution (0.19 M) of EDTMP was added (the pH of the aqueous solution of EDTMP was adjusted to 8.5 with concentrated ammonia to promote the complete dissolution of EDTMP). The reaction medium turned orange. The heating was stopped after 20 min, but the stirring was maintained until the medium returned to room temperature. The final solution obtained was stored in a Schlenk tube under argon (7° C).

2.2.4. Functionalization of the silver nanoparticles. 160 µL (3.2 µmol) of an aqueous solution of 4SHPy were added to 20 mL (approximately 0.001 µmol of NPs) of the solution of AgNPs

obtained above. The mixture was placed under magnetic stirring for 16 h at room temperature. The initial orange color of AgNPs changed to brick red with the addition of 4SHPy, then remained constant until stirring was complete. The solution was stored under argon at 7° C. An aliquot (10 mL) was centrifuged, 8 mL of supernatant was taken and 8 mL of Milli-Q water added. A new centrifugation cycle was performed. The operation was repeated 3 times. In the last cycle, 8 mL of supernatant were taken out and the remaining solution was lyophilized. About 4 mg of a black powder was isolated.

2.2.5. Preparation of the hybrid [FePc-4SHPy@AgNPs]. To 10 mL of the 4SHPy@AgNPs solution described above, 1 mL of a solution of FePc in DMSO (2 μmol) was added; then the mixture was stirred for 72 h at room temperature. The initial colors, blue for FePc and brick red for 4SHPy@AgNPs, changed over time until a mixture of green color was obtained. This solution was stored under argon at 7° C. As for the functionalized particles, an aliquot of the solution was taken out, purified by centrifugation and then lyophilized before analysis. About 5 mg of compound was isolated as a black powder.

2. 3. Characterization

2.3.1. Optical absorption spectroscopy. UV-visible spectra were recorded using a 190 DES (Double Energy System) type spectrometer from compounds dissolved in a suitable solvent (water or DMSO).

2.3.2. Infrared absorption spectroscopy. IR spectra were recorded using a Brucker TENSOR 27, ATR diamond type spectrometer from the powders of the samples.

2.3.3. Transmission Electron Microscopy (TEM). The study was carried out at Centre de Microcaractérisation Raimond Castaing (Toulouse). Conventional TEM images were recorded on a JEOL JEM 1400 microscope. Higher resolution images were recorded on a JEOL JEM ARM200F Cold FEG microscope with an acceleration voltage of 200 kV, Cs corrector on the probe, and EDX analyzer, in STEM - HAADF mode for imaging. Samples were prepared by depositing a drop of the diluted colloidal solution on a copper grid covered with a thin film of carbon, followed by air drying and then drying under high vacuum. A beamshower (30-minutes) was applied to eliminate residual carbon pollution. Average sizes were determined after counting a minimum of 250 particles using Image J software. The size distribution was fitted by a Gaussian law and results are given as the mean size ± sigma.

3. Results and discussions

The formation of the hybrid species was studied by following these steps: first, the FePc complex was synthesized and its reactivity towards 4SHPy was investigated (**Scheme** 1); second, Ag NPs were prepared then functionalized with 4SHPy. The hybrid species was finally obtained by reacting the FePc complex with the functionalized nanoparticles as depicted in **Scheme** 2.

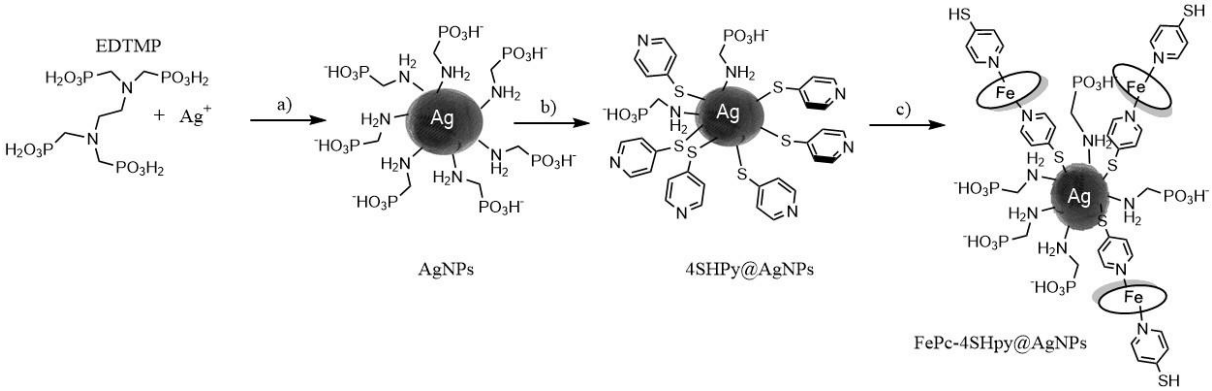

Scheme 2. Synthetic pathway towards the hybrid material. a) water, pH = 8.5, reflux, 30 min.; b) water, 4-thiopyridine, r.t., 16 h; c) water/DMSO (10/1 v/v), FePc, 72 h

3. 1. The complex FePc(4SHPy)$_2$

Firstly, we prepared the FePc(4SHPy)$_2$ complex (**Scheme** 1) to assess the reactivity of FePc with 4SHPy. Addition of a 10 fold excess of 4SHPy to FePc in acetonitrile and 15 hours reflux, a green solid could be recovered in very good yield (90%). The product was first studied by infra-red (IR) spectroscopy in attenuated total reflexion (ATR) mode. Its low frequency IR spectrum (100-600 cm^{-1}) has a better resolution compared to that of FePc (Fig. 1). This result can be explained by the coordination of the axial ligands which would have caused a reorganization of the complex in the solid state. The band at 435 cm^{-1} was attributed by Bayo K to the metal-isoindole ligand vibration of the phthalocyanine macrocycle. The latter, through a study on FePc carrying a series of pyridine ligands has shown that this band is only modified when the macrocycle carries substituents at the periphery [29, 30]. Accordingly this band is observed here in the two spectra with the same intensity, as the only modification is expected to occur on the metal center. Nakamoto K and al., by studying a series of metal complexes (Ni, Cu, Zn) coordinated with imidazole, have shown that the vibration band of the metal-nitrogen bond with the ligand is observed between 325 cm^{-1} and 210 cm^{-1} [32]. We attribute, by analogy, the new band which appears at 270 cm^{-1} in the IR

spectrum of the complex $FePc(4SHPy)_2$ to the Fe-N vibration band of the metal-ligand (Fe-4SHPy) bond.

We note the presence of the new band at 545 cm^{-1} which we attribute to the vibration band of the S-S disulfide bond which may arise from the partial oxidation of the 4SHPy. The study of the IR spectrum of the green product recovered thus brings first indications of the formation of the $FePc(4SHPy)_2$ complex.

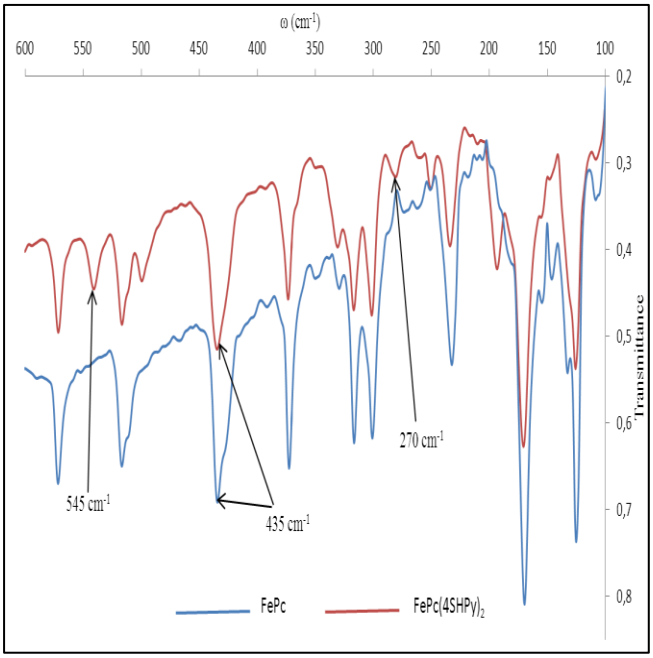

Fig. 1 Infrared spectrum of $FePc(4SHPy)_2$ in comparison with that of FePc

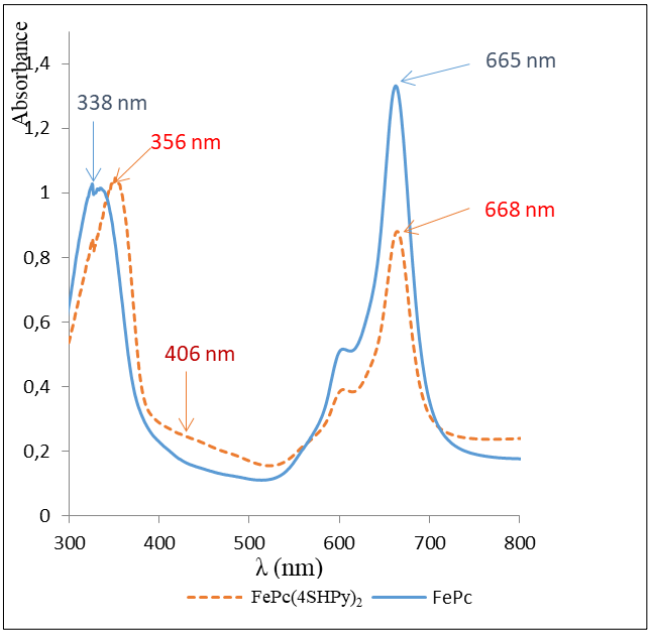

Fig. 2 UV-Visible spectrum of $FePc(4SHPy)_2$ in comparison with that of FePc in DMSO.

The optical absorption spectrum of the reaction compound in DMSO (Fig. 2), is characterized in the UV-visible region by modifications already observed in the spectra of $FePc(PyR)_2$ (R= 4OHPy, 3OHPy, 3ClPy, 3CNPy, 4CNPy, 3MePy, 4MePy) complexes which are hexacoordinate complexes of FePc [27, 28]. These modifications, which are in particular the appearance of the charge transfer band around 400 nm as well as the bathochromic shift of the electronic absorption bands of the complex, confirm the formation of the $FePc(4SHPy)_2$ complex. Likewise, the results of elemental analysis [Cal: C/N = 3.5; H/N = 0.17; C/S = 13.86 and Exp: C/N = 3.55; H/N = 0.14; C/S = 15.6] are in agreement with the proposed formula, $FePc(4SHPy)_2$: a hexacoordinated complex in which the thiopyridine ligand is axially attached to the iron center on either side of the plane of the macrocycle. The thiol function (-SH) being free, the formation of disulfide bridges can be expected upon partial oxidation as suggested by the IR spectrum. This study thus confirms the chemioselectivity of the coordination on the Fe^{2+} center of the FePc that follows the simple HSAB principle in this case: coordination of the hard pyridine base is favored over that of the soft sulfur atom on the first raw transition metal ion that is Fe^{2+}. To the best of our knowledge this complex was never prepared before. As it displays pendant thiol/sulfide bonds, it could be used as a scaffold to build new polymetallic coordination complexes or other adducts.

Here, we took profit of this reactivity to connect FePc with 4SHPy@AgNPs. (see below)

3. 2. Silver nanoparticles

AgNPs were prepared by reduction of silver nitrate by ethylenediaminetetramethylene-phosphonic acid (in 1/1 molar ratio) in water, at reflux for 30mn. It is assumed, based on previous literature reports, that the aminomethylphosphonate that forms *in situ* acts as a stabilizing agent leading to a stable colloidal suspension (Scheme 2, step a). [31] It is noteworthy that the reaction is carried out at pH =8.5, to avoid protonation of the aminomethylphosphonate. In this way, with the NH_2 function being coordinated to the surface of the AgNPs, the pendant phosphonate group affords a negative surface charge that contribute to the colloidal stability of the AgNPs in solution due to electrostatic repulsions. The UV-visible spectrum (Fig. 3) of the yellow solution obtained shows a narrow band with an absorption maximum around 400 nm characteristic of the surface plasmon resonance band of quasi spherical AgNPs [31, 33-34]. Their purification by dialysis with Milli Q water (twice 3 h then 15 h), in order to remove the excess of ionic species, changes the position of the absorption band very little (λ_{max} = 396 nm). The results obtained by TEM confirm that the nanoparticles are quasi spherical, and allow determining their average size: 17 ± 4 nm (Fig. 4). This size is in line with the size of the AgNPs studied for their antibacterial properties [24]. Interestingly it is larger than the size of the AgNPs used by e.g. Masilela N and al. [25] (*ca.* 8 nm), or Nakonieczna J and al. (*ca.* 5 nm) [35] when designing photoactivable AgNPs based bactericides. As the redox potential of AgNPs increases with size [36], it is believed that the release of Ag^+ ions would be slower and thus more progressive with the larger NPs prepared in our work, affording a longer lasting effect against bacteria.

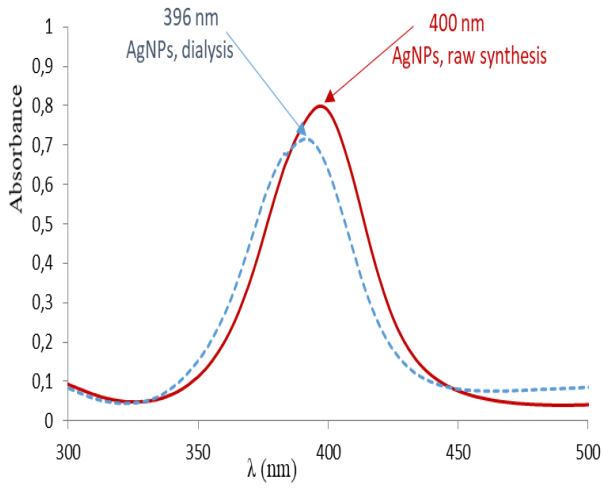

Fig. 3 UV-Visible absorption spectra of AgNPs before and after dialysis in aqueous medium.

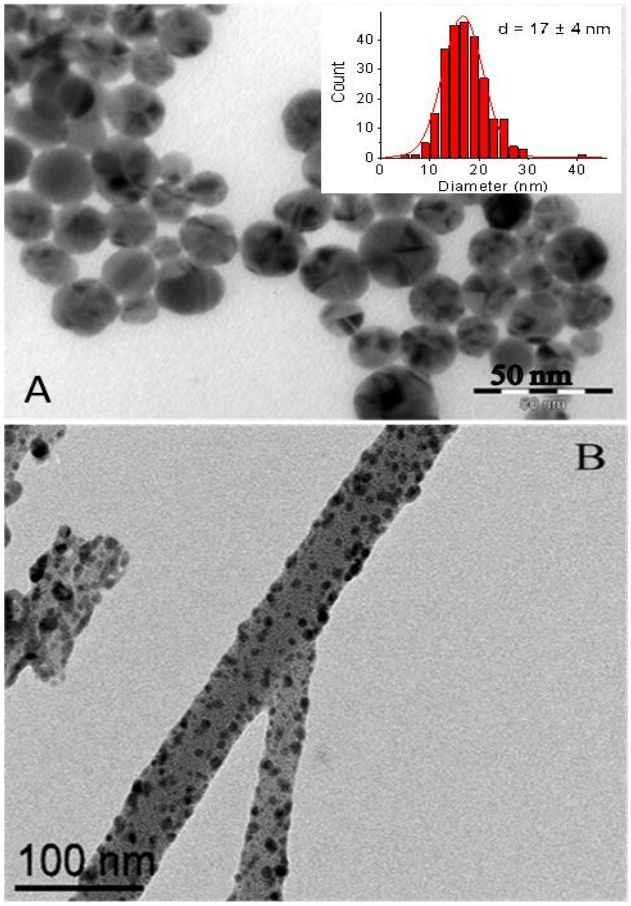

Fig. 4 TEM images of (A) AgNPs and corresponding size histogram in insert) and (B) 4SHPy@AgNPs

3. 3. Nanoparticles functionalized by 4-thiopyridine (4SHPy@AgNPs)

The aqueous dispersion of the AgNPs described above was reacted with 4SHPy at room temperature to verify the reactivity of 4SHPy towards AgNPs (Scheme 2, step b). Given the size of the NPs, we assumed that only 10% of the silver atoms were accessible for surface coordination and introduced ≈ 1.1 eq of 4SHPy per surface silver atom. The comparison of the results of the spectroscopic analyzes obtained from the reference 4SHPy and the AgNPs, native or after reaction with 4SHPy, are in agreement with the coordination of the thiol at the surface of the particles. Thus, the vibration band of the –SH bond at 2620 cm^{-1} is no longer observed on the IR spectrum of the functionalized AgNPs while the other vibrations characteristic of 4SHPy are indeed present, which suggests coordination by formation of a surface thiolate [25] (Fig. 5). In UV-visible spectroscopy, the characteristic absorption band of 4SHPy undergoes a hypsochromic effect (326 nm to 302 nm) in accordance with its coordination at the surface of AgNPs, while the characteristic absorption band of AgNPs

undergoes a bathochromic effect (Fig. 6) of about 15 nm, which is also in agreement with a functionalization of their surface.

However, this shift to longer wavelengths is accompanied by a widening of the peak which suggests a change in the organization of the nanoparticles in solution [34, 37].

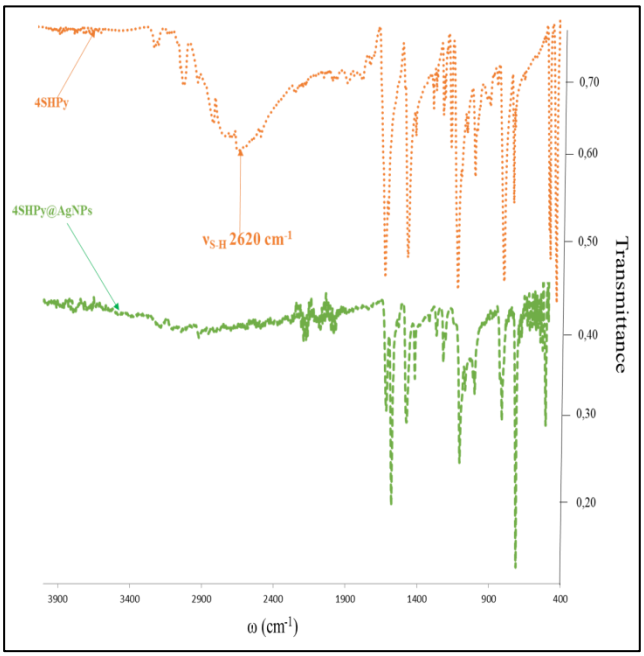

Fig. 5 Infrared spectra of 4SHPy and 4SHPy@AgNPs

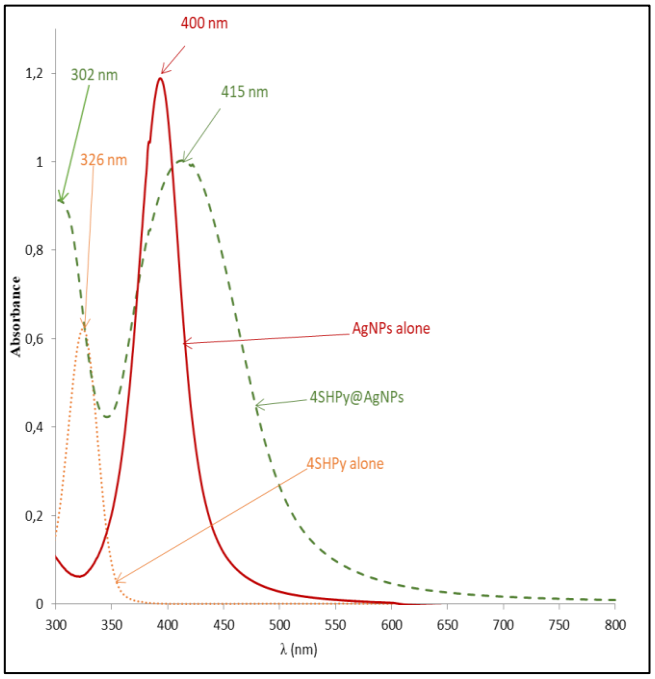

Fig. 6 UV-Visible absorption spectra of AgNPs, 4SHPy@AgNPs and 4SHPy in aqueous medium

TEM images (Fig. 4, B) indeed show that the nanoparticles assemble along filaments of less dense material whose composition has not been identified. This result is at first surprising. Coordination of 4SHPy by its S atom should indeed expose the pyridine function which has a good affinity with water, thus leading to a good dispersion of the NPs. However coordination of 4SHPy on the surface should substitute, at least partially, aminomethylphosphonate ligands (as depicted Scheme2, step b) thus decreasing the surface charges and associated repulsive electrostatic forces, which might ease the organization of the NPs into dense patterns. Another probable explanation is that there could be ″π-π stacking″ phenomena between aromatic nuclei which would promote the observed stackings, as observed *e.g.* for coumarine stabilized AgNPs [38] and/or also hydrogen bonds could form between the nitrogen of the pyridine and the free $–NH_2$ functions of the aminomethylphosphonate ligands released in the basic medium. Anyway the results all point towards the successful coordination of 4SHPy onto the AgNPs via the S atom, leaving the pyridine function free for further reaction, here with FePc.

3. 4. Hybrid [FePc-4SHPy@AgNPs]

The functionalized 4SHPy@AgNPs were subsequently reacted with FePc (Scheme 2, step c). The IR spectrum of the hybrid system obtained by reacting FePc with the functionalized AgNPs (4SHPy@AgNPs) shows the characteristic bands of FePc (Fig. 7) as well as those of 4SHPy. However, we do note in the spectrum of the hybrid complex notable changes such as the disappearance of certain vibration bands and the emergence of new ones.

In the spectrum of the hybrid compound, we observe the absence of the band at 443 cm^{-1}, observed in the spectrum of FePc. Also the splitting of the vibration bands between 770 and 780 cm^{-1} which is clearly observed in the spectrum of FePc is no longer evident in that of the hybrid compound. The band observed at 545 cm^{-1} in the spectrum $FePc(4SHPy)_2$ and attributed to a S-S vibration is not observed in the spectrum of the hybrid compound. In fact, in the spectrum of the complex $FePc(4SHPy)_2$, the thiol functions being free, they can form disulfide bridges. In contrast, the thiol function is quenched by coordination on the AgNPs. The absence of the S-S vibrations in the IR spectrum of the hybrid compound is therefore in agreement with the formation of the expected compound and stability of the Ag-S bond (no thiol release nor disulfide formation during the reaction with FePc) [39, 40].

Between 1000 and 1800 cm^{-1}, the notable modifications are mainly modulations of the relative intensities of the bands in the spectrum of the hybrid compared to the spectra of the references.

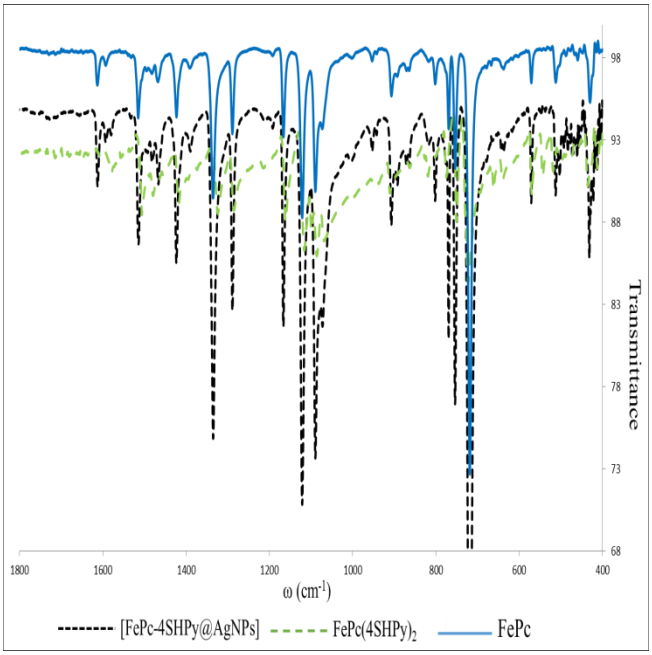

Fig. 7 Infrared spectra of $FePc(4SHPy)_2$, [FePc-4SHPy@AgNPs] and FePc

The UV-Visible absorption spectrum of the reaction product between 4SHPy@AgNPs and FePc essentially shows three transition bands (at 416 nm, and 610 nm and 671 nm) (Fig. 8), characteristic respectively of AgNPs and of FePc. It is noteworthy that the plasmonic absorption band (at 416 nm) is narrower after reaction of the functionalized AgNPs with FePc, suggesting that the NPs are less aggregated. There is a bathochromic shift of the Q band of the FePc complex which goes from 665 nm to 671 nm. This shift could be explained by the fact that the AgNPs are rich in electrons, and would contribute to increasing the electron density on the phthalocyanine macrocycle. The Q band of the hybrid is also thinner than that of the reference FePc, which indicates the disappearance of the aggregates [25].

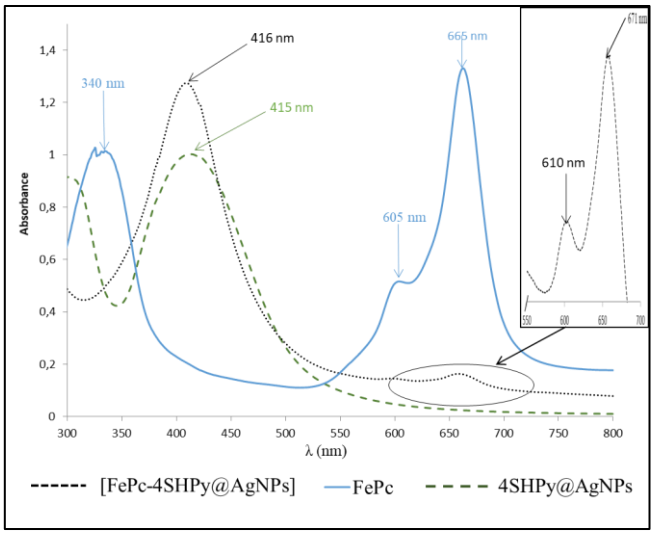

Fig. 8 UV-Visible absorption spectra of [FePc-4SHPy@AgNPs], 4SHPy@AgNPs and FePc (insert: 6 fold enlargement of the [FePc-4SHPy@AgNPs] spectrum highlighting the main absorption bands of FePc)

Contrarily to what was observed for the $FePc(4SHPy)_2$ sample, the characteristic charge transfer band of the Fe-Py bond is not observed due to the intense absorption of the nanoparticles in the same area of the spectrum (Fig. 8). Spectroscopic studies alone therefore do not allow concluding on the coordination of the phthalocyanine.

On the other hand, the TEM study of the hybrid shows the disappearance of the assemblies obtained previously (Fig. 9), in perfect agreement with the narrowing of the plasmonic and Q absorption bands discussed above. This can be interpreted as evidence of the coordination of the phthalocyanine on the 4SHPy@AgNPs. The π-π interactions between aromatic rings are then considerably attenuated. The EDX analysis of a region of the TEM grid presenting a high density of NPs shows the presence of silver, phosphorus, sulfur, and iron (Fig. 10). The phosphorus contribution indicates that some aminomethylphosphonic acid, formed *in situ* during the synthesis of the AgNPs and that stabilizes the initial AgNPs, is still present at the surface of the AgNPs in the hybrid system, as depicted in Scheme 2. The presence of sulfur confirms that 4SHPy was indeed coordinated at the surface, even if it did not displace all aminomethylphosphonic acid ligands. The low intensity of the iron signal indicates a low quantity of iron phthalocyanine in the hybrid system compared to silver, in agreement with the presence of the complexes only at the surface of the AgNPs. It correlates well with the position of the plasmonic absorption band that was not modified upon coordination of the FePc, indicating that the dielectric constant of the medium surrounding the AgNPs was not significantly altered.

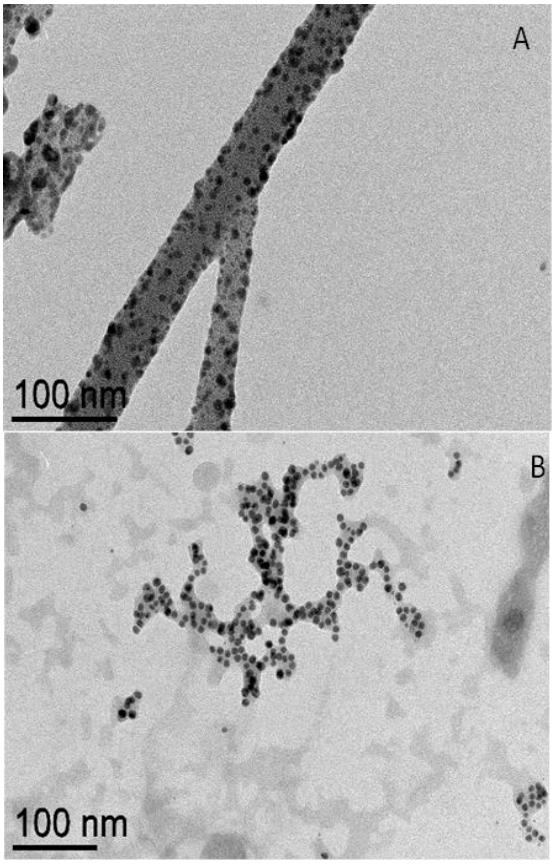

Fig. 9 TEM images of 4SHPy@AgNPs (A) and [FePc-4SHPy@AgNPs] (B)

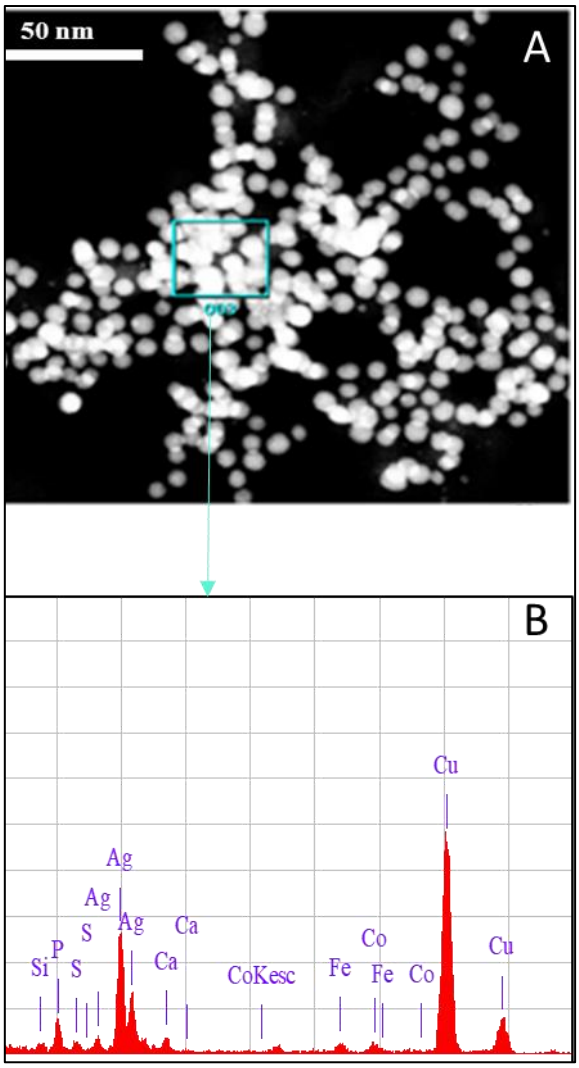

Fig. 10 EDX analysis (B) of the hybrid species carried out on the boxed area in the STEM-HAADF image (A) (scale bar = 50 nm)

Moreover, EDX analysis of regions of the TEM grid outside the matrix only highlights the components of the carbon grid (Fig. SI 1). This further confirms that the complex is found only in immediate vicinity of the surface of the AgNPs. The above observations thus indicate that a robust FePc-4SHPy@AgNPs hybrid system could be synthesized and isolated.

4 Conclusions

The hybrid species [FePc-4SHPy@AgNPs] has been synthesized and isolated for the first time. It exhibits notable modifications in absorption spectroscopy compared to the two initial entities, AgNPs and FePc: bathochromic displacement of around 15 nm of the plasmonic band of Ag and hypsochromic displacement of the absorption band of the complex. These results, indicative of a modification of the surface of AgNPs, are in agreement with those of the literature [33, 39-41].

The results obtained from the infrared analysis suggest that the expected reactions have been carried out. Indeed, the vibration band of the S-H bond of 4SHPy at 2630 cm^{-1} is absent from the spectrum of 4SHPy@AgNPs; which is a consequence of the reaction between AgNPs and 4SHPy. Likewise, the band which appears at 545 cm^{-1} in the spectrum of $FePc(4SHPy)_2$ and attributable to S-S vibration is no longer observed in the spectrum of the hybrid complex. We can therefore deduce that the expected compound was formed.

TEM images show, one of the rare times, nanoparticles associated with phthalocyanine complexes better dispersed in solution. This could be explained by the presence of the axial ligand which creates steric hindrance thus reducing the phenomenon of aggregation, in agreement with the narrowing of the Q band of the complex. The EDX analyzes attest the presence of the various ligand atoms on the surface of the nanoparticles. These results argue in favor of a good coordination of phthalocyanines at the surface of nanoparticles which validates our synthesis strategy.

We believe that we can, through this species FePc-AgNP hybrid, combine the individual properties of each of the components (cooperative effects) but also obtain new properties (synergistic effects); which could be an asset for antibacterial applications. We next plan to test the antibacterial activity of the synthesized hybrid against the bacteria of *Escherichia coli* and *Staphylococcus aureus* which are harmful bacteria frequently encountered.

Acknowledgements

The authors thank the CNRS and the Paul-Sabatier University for their financial support, Centre de Microcaractérisation Raimond Castaing for access to the microscopes. They would like to thank Joseph KI ZERBO University, Paul-Sabatier University and particularly the SCAC-French Embassy in Ouagadougou, Burkina Faso for their help in carrying out this work.

Compliance with Ethical Standards

Conflict of interest The authors declare that they have no confict of interest.

References

1. Braun A, Tcherniac J (1907) Uber die Produckte der Einwirkung von Acetanhydrid auf Phthalamid. Ber. Deutsch. Chem. Ges. 40: 2709-2714.

2. Gregory P (2000) Industrial applications of phthalocyanines. J Porphyr Phthalocyanines 4: 432–437.

3. Ogunsipe A, Nyokong T (2004) Effects of substituents and solvents on the photochemical properties of zinc phthalocyanine complexes and their protonated derivatives. J Mol Struct 689: 89–97.

4. Ogura S, Tabata K, Fukushima K, Kamachi T, Okura I (2006) Development of phtalocyanines for photodynamic therapy. J Porphyr Phtalocyanines 10: 1116-1124.

5. Nyokong T, Bedioui F (2006) Self-assembled monolayers and electropolymerized thin films of phthalocyanines as molecular materials for electroanalysis. J Porphyr Phthalocyanines 10: 1101-1115.

6. Rawling T, Austin C, Buchholz F, Colbran SB, McDonagh AM (2009) Ruthenium phthalocyanine-bipyridyl dyads as sensitizers for dye-sensitized solar cells: Dye coverage versus molecular efficiency. Inorg Chem 48: 3215-3227.

7. Sakamoto K, Ohno-Okumura E (2009) Syntheses and functional properties of phthalocyanines. Materials 2: 1127-1179.

8. Güzel E, Koçyiğit ÜM, Taslimi P, Erkan S, Taskin OS (2021) Biologically active phthalocyanine metal complexes: Preparation, evaluation of α-glycosidase and anticholinesterase enzyme inhibition activities, and molecular docking studies. Biochem Mol Toxicol 35: 1-9.

9. Ahmetali E, Atmaca GY, Karaoğlu HP, Erdoğmuş A, Koçak MB (2019) Photophysical and photochemical properties of newly synthesized zinc(II) and chloroindium(III)phthalocyanines substituted with 3,5-bis(trifluoromethyl)phenoxy groups. J Porphyr Phthalocyanines 23: 960–968.

10. Martins TJ, Negri LB, Pernomian L, Faial KCF, Xue C, Akhimie RN, Hamblin MR, Turro C, da Silva RS (2021) The Influence of Some Axial Ligands on Ruthenium–Phthalocyanine Complexes: Chemical, Photochemical, and Photobiological Properties. Front Mol Biosci 7: 1-12.

11. Kulu I, Mantareva V, Kussovski V, Angelov I, Durmuş M (2022) Effects of metal ion in cationic Pd(II) and Ni(II) phthalocyanines on physicochemical and photodynamic inactivation properties. J Mol Struct 1247: 131288.

12. Mantareva VN, Kussovski V, Orozova P, Dimitrova L, Kulu I, Angelov I, Durmus M, Najdenski H (2022) Photodynamic Inactivation of Antibiotic-Resistant and Sensitive Aeromonas hydrophila with Peripheral Pd(II)- vs. Zn(II)-Phthalocyanines. Biomedicines, 10: 384.

13. Amitha GS, Vasudevan S (2022) Optical and electrochemical properties of peripherally substituted chromium and manganese phthalocyanines. Polyhedron 212: 115591.

14. Lokesh KS, Narayanan V, Sampath S (2009) Phthalocyanine macrocycle as stabilizer for gold and silver nanoparticles. Microchim Acta 167: 97-102.

15. Fashina A, Antunes E, Nyokong T (2013) Characterization and photophysical behavior of phthalocyanines when grafted onto silica nanoparticles. Polyhedron 53: 278–285.

16. Vior MCG, Awruch J, Dicelio LE, Diz VE (2019) 2(3), 9(10), 16(17), 23(24)-tetrakis[(3-mercapto)propoxy]phthalocyaninate zinc (II)/gold nanoparticle conjugates: Synthesis and photophysical properties. J Photochem Photobiol A 368: 242–247.

17. Mgidlana S, Sen P, Nyokong T (2022) Photodegradation of tetracycline by asymmetrical zinc(II)phthalocyanines conjugated to cobalt tungstate nanoparticles. J Mol Struct 1261: 132938-132947.

18. Pinto BCS, Ambrósio JAR, Marmo VLM, Pinto JG, Raniero LJ, Ferreira-Strixino J, Simioni AR, Beltrame M (2022) Synthesis, characterization, and evaluation of chloroaluminium phthalocyanine incorporated in poly(ε-caprolactone) nanoparticles for photodynamic therapy. Photodiagnosis Photodyn Ther 38: 102850-132858.

19. Abbasi E, Milani M, Aval SF, Kouhi M, Akbarzadeh A, Nasrabadi HT, Nikasa P, Joo SW, Hanifehpour Y, Nejati-Koshki K, Samiei M (2016) Silver nanoparticles: Synthesis methods, bio-applications and properties. Crit Rev Microbiol 42: 173-180.

20. Dilshad E, Bibi M, Sheikh NA, Tamrin KF, Mansoor Q, Maqbool Q, Nawaz M (2020) Synthesis of Functional Silver Nanoparticles and Microparticles with Modifiers and Evaluation of Their Antimicrobial, Anticancer, and Antioxidant Activity. J Funct Biomater 11: 76-96.

21. Vinodhini S, Vithiya BSM, Prasad TAA (2022) Green synthesis of silver nanoparticles by employing the Allium fistulosum, Tabernaemontana divaricate and Basella alba leaf extracts for antimicrobial applications. J. King Saud Univ. Sci. 34: 101939-101947.

22. Le A-T, Huy PT, Tam PD, Huy TQ, Cam PD, Kudrinskiy AA, Krutyakov YA (2010) Green synthesis of finely-dispersed highly bactericidal silver nanoparticles via modified Tollens technique. Curr Appl Phys 10: 910-916.

23. Shrivastava S, Bera T, Singh SK, Singh G, Ramachandrarao P, Dash D (2009) Characterization of antiplatelet properties of silver nanoparticles. ACS Nano 3: 1357-1364.
24. Zheng K, Setyawati MI, Leong DT, Xie J (2018) Antimicrobial silver nanomaterials. Coord Chem Rev 357: 1–17
25. Masilela N, Antunes E, Nyokong T (2013) Axial coordination of zinc and silicon phthalocyanines to silver and gold nanoparticles: an investigation of their photophysicochemical and antimicrobial behavior. J Porphyr Phthalocyanines 17: 417–430.
26. Ogunsipe A, Maree D, Nyokong T (2003) Solvent effects on the photochemical and fluorescence properties of zinc phthalocyanine derivatives. J Mol Struct 650: 131–140.
27. Bayo K, Saba A, Ouédraogo GV, Terzian G, Benlian D (1992) Dérivés substitués de la ferrophtalocyanine. J Mol Struct 271: 19-26
28. Zanguina A, Bayo-Bangoura M, Bayo K, Ouédraogo GV (2002) IR and UV-visible spectra of iron (II) phthalocyanine complexes with phosphine or phosphate. Bull Chem Soc Ethiop 16: 73-79.
29. (a) Chen Y, Hanack M, Blau WJ, Dini D, Liu Y, Lin Y, Bai J (2006) Soluble axially substituted phthalocyanines: Synthesis and nonlinear optical response. Mat Sci 41: 2169-2185 (b) Kadish KM, Smith KM, Guilard R, Flom SR (2003) The Porphyrin Handbook; Academic Press: New York 19: 179–190.
30. Ouédraogo GV, More C, Richard Y, Benlian D (1981) Charge-transfer and Mössbauer spectra of axially substituted iron phthalocyanines. Inorg Chem 20: 4387-4393.
31. Chaikin Y, Bendikov TA, Cohen H, Vaskevich A, Rubinstein I (2013) Phosphonate-stabilized silver nanoparticles: one-step synthesis and monolayer assembly. J Mater Chem C 1: 3573-3583.
32. Nakamoto K (1970) Infrared and Raman spectra of Inorganic and coordination compounds. 2nd ed Wiley Interscience, New-York.
33. Mamdouh S, Mahmoud A, Samir A, Mobarak M, Mohamed T (2022) Using femtosecond laser pulses to investigate the nonlinear optical properties of silver nanoparticles colloids in distilled water synthesized by laser ablation. Physica B: Physic of Condensed Matter 631: 413727-413736.
34. Taleb A, Petit C, Pileni MP (1997) Synthesis of highly monodisperse silver nanoparticles from AOT reverse micelles: A way to 2D and 3D self-organization. Chem Mater 9: 950-959.
35. Nakonieczna J, Rapacka-Zdonczyk A, Kawiak A, Bielawski KP, Grinholc M (2013) Sub-lethal photodynamic inactivation renders Staphylococcusaureus susceptible to silver Nanoparticles. Photochem. Photobiol. Sci. 12: 1622–1627.

36. Khatouri J, Mostafavi M, Amblard J, Belloni J (1993) Ionization potential of clusters in liquids. Z Phys D - Atoms, Molecules and Clusters 26: 82–86.
37. Shenashen MA, El-Safty SA, Elshehy EA (2014) Synthesis, Morphological Control, and Properties of Silver Nanoparticles in Potential Applications. Part Part Syst Charact 31: 293–316.
38. Paul S, Chakraborty BB, Anwar S, Paul SB, Choudhury S (2020) Self-assembly of silver nanoparticles through functionalization with coumarin-thiazole fused-ring thiol. Heliyon 6: 03674-03679.

39. Forteath S, Antunes E, Chidawanyika W, Nyokong T (2012) Unquenched fluorescence lifetime for b-phenylthio substituted zinc phthalocyanine upon conjugation to gold nanoparticles. Polyhedron 34: 114–120

40. Oluwole DO, Yagodin AV, Britton J, Martynov AG, Gorbunova YG, Tsivadze AY, Nyokong T (2017) Optical limiters with improved performance based on nanoconjugates of thiol substituted phthalocyanine with CdSe quantum dots and Ag nanoparticles. Dalton Trans. 46: 16190–16198.
41. Stuart BH (2004) Infrared spectroscopy: fundamentals and applications, John Wiley & Sons, England.

Supporting information

to

Synthesis and study of the physicochemical properties of a hybrid species: iron phthalocyanine-silver nanoparticles

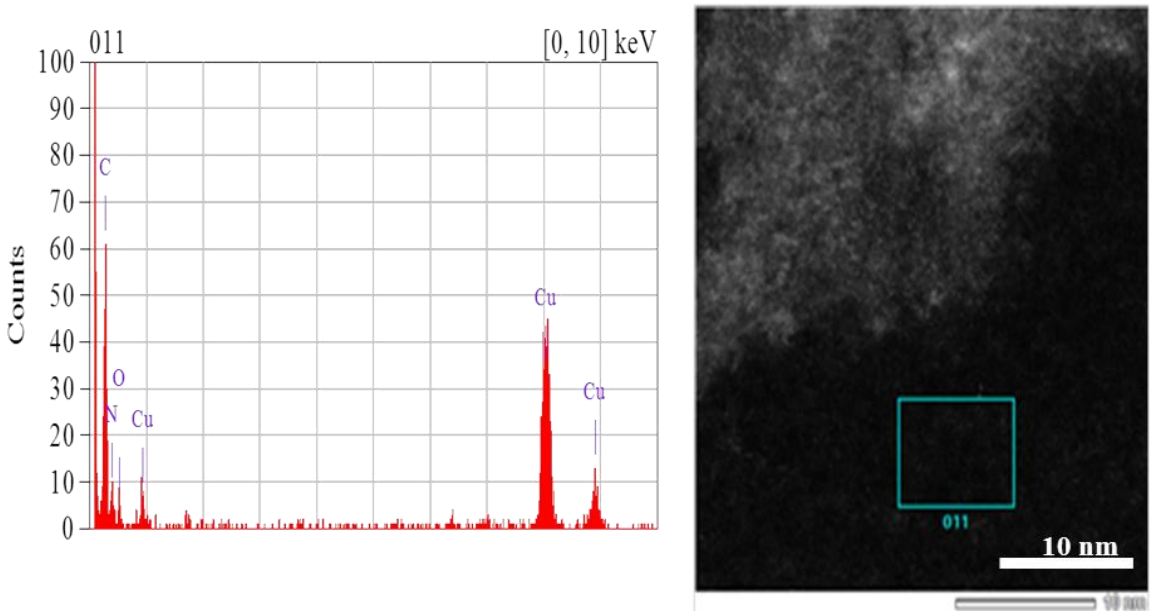

Fig. SI 1: EDX analysis of the boxed area on the right image (scale bar =10 nm) and corresponding to the matrix surrounding the hybrid species